

## Magnetic and Electronic Properties of $\text{CaCu}_3\text{Cr}_4\text{O}_{12}$ and $\text{CaCu}_3\text{Cr}_2\text{Sb}_2\text{O}_{12}$ by First-Principles Density Functional Calculation

H. P. Xiang,<sup>†‡</sup> X. J. Liu,<sup>†</sup> E. J. Zhao,<sup>†‡</sup> J. Meng,<sup>†</sup> and Z. J. Wu<sup>\*†</sup>

Key Laboratory of Rare Earth Chemistry and Physics, Changchun Institute of Applied Chemistry, Chinese Academy of Sciences, Changchun 130022, P.R. China, Graduate School, Chinese Academy of Sciences, Beijing 100049, P.R. China

Received February 5, 2007

The electronic and magnetic properties of  $\text{CaCu}_3\text{Cr}_4\text{O}_{12}$  and  $\text{CaCu}_3\text{Cr}_2\text{Sb}_2\text{O}_{12}$  are investigated by the use of the full-potential linearized augmented plane wave (FP-LAPW) method. The calculated results indicate that  $\text{CaCu}_3\text{Cr}_4\text{O}_{12}$  is a ferrimagnetic and half-metallic compound, in good agreement with previous theoretical studies.  $\text{CaCu}_3\text{Cr}_2\text{Sb}_2\text{O}_{12}$  is a ferrimagnetic semiconductor with a small gap of 0.136 eV. In both compounds, because  $\text{Cr}^{4+}$  3d ( $d^2$ ) and  $\text{Cr}^{3+}$  3d ( $d^3$ ) orbitals are less than half filled, the coupling between Cr–Cu is antiferromagnetic, whereas that between Cu–Cu and Cr–Cr is ferromagnetic. The total net spin moment is 5.0 and 3.0  $\mu_B$  for  $\text{CaCu}_3\text{Cr}_4\text{O}_{12}$  and  $\text{CaCu}_3\text{Cr}_2\text{Sb}_2\text{O}_{12}$ , respectively. In  $\text{CaCu}_3\text{Cr}_4\text{O}_{12}$ , the 3d electrons of  $\text{Cr}^{4+}$  are delocalized, which strengthens the Cr–Cr ferromagnetic coupling. For  $\text{CaCu}_3\text{Cr}_2\text{Sb}_2\text{O}_{12}$ , the doping of nonmagnetic ion  $\text{Sb}^{5+}$  reduces the Cr–Cr ferromagnetic coupling, and the half-filled  $\text{Cr}^{3+}$   $t_{2g}$  ( $t_{2g}^3$ ) makes the chromium 3d electrons localized. In addition, the ordering arrangement of the octahedral chromium and antimony ions also prevents the delocalization of electrons. Hence,  $\text{CaCu}_3\text{Cr}_2\text{Sb}_2\text{O}_{12}$  shows insulating behavior, in agreement with the experimental observation.

### I. Introduction

In the ideal perovskite  $\text{ABO}_3$ , where the octahedra are not tilted, the structure is cubic, with coordination numbers of 12 and 6 for A and B cations, respectively. Nonetheless, significant deviation from the ideal stoichiometry and structure frequently occurs. The tilting of the  $\text{BO}_6$  octahedra, where some or all of the B–O–B angles are bent away from  $180^\circ$ , is the major distortion in perovskite compounds. To accommodate the tilting, the coordination number of three-quarters of the A cations will be decreased from 12 to 4, by forming a square-planar coordination. This gives the  $\text{AA}'_3\text{B}_4\text{O}_{12}$  structure. It is cubic, with coordination numbers of 12, 6, and 4 for A, B, and A', respectively. In recent years, the complex perovskite compound  $\text{AA}'_3\text{B}_4\text{O}_{12}$  has attracted a great deal of attention in both experimental and theoretical studies as a result of their interesting and unexpected properties. For instance, the hybrid cupromanganite  $\text{CaCu}_3\text{-Mn}_4\text{O}_{12}$  shows a quite-large magnetoresistance (up to several tens of percent) at a relatively low magnetic field over a wide temperature range.<sup>1</sup> The complex perovskite  $\text{CaCu}_3\text{-$

$\text{Ti}_4\text{O}_{12}$  has been reported as having the largest dielectric constant ( $\epsilon' = 10^5$ ) over a wide temperature range (from 100 to 600 K) ever measured.<sup>2–4</sup> In addition, it is interesting to find the valence degeneracy between copper and ruthenium in  $\text{CaCu}_3\text{Ru}_4\text{O}_{12}$  due to the broadening of ruthenium 4d band.<sup>5</sup> On the other hand, to improve the properties of  $\text{AA}'_3\text{B}_4\text{O}_{12}$ , B can be replaced by 50% B', resulting in a new perovskite  $\text{AA}'_3\text{B}_2\text{B}'_2\text{O}_{12}$ .<sup>6–9</sup> It is well-known that the properties of  $\text{A}_2\text{BB}'\text{O}_6$  or  $\text{AA}'\text{BB}'\text{O}_6$  perovskites are very sensitive to the properties (i.e., size, electronegativity, and electronic configuration) of B and/or B' cations and their

- (1) Zeng, Z.; Greenblatt, M.; Subramanian, M. A.; Croft, M. *Phys. Rev. Lett.* **1999**, *82*, 3164.
- (2) Subramanian, M.; Li, D.; Reisner, B.; Sleight, A. *J. Solid State Chem.* **2000**, *151*, 323.
- (3) Ramirez, A. P.; Subramanian, M. A.; Gardel, M.; Blumberg, G.; Li, D.; Vogt, T.; Shapiro, S. M. *Solid State Commun.* **2000**, *115*, 217.
- (4) Homes, C.; Vogt, T.; Shapiro, S.; Wakimoto, S.; Ramirez, A. *Science* **2001**, *293*, 673.
- (5) Subramanian, M. A.; Sleight, A. W. *Solid State Sci.* **2002**, *4*, 347.
- (6) Byeon, S.-H.; Lufaso, M. W.; Parise, J. B.; Woodward, P. M.; Hansen, T. *Chem. Mater.* **2003**, *15*, 3798.
- (7) Byeon, S.-H.; Lee, S.-S.; Parise, J. B.; Woodward, P. M.; Hur, N. H. *Chem. Mater.* **2004**, *16*, 3697.
- (8) Byeon, S.-H.; Lee, S.-S.; Parise, J. B.; Woodward, P. M.; Hur, N. H. *Chem. Mater.* **2005**, *17*, 3552.
- (9) Byeon, S.-H.; Lee, S.-S.; Parise, J. B.; Woodward, P. M. *Chem. Mater.* **2006**, *18*, 3873.

\* To whom correspondence should be addressed. Email: zjwu@ciac.jl.cn. Fax: +86-431-85698041.

<sup>†</sup> Changchun Institute of Applied Chemistry.

<sup>‡</sup> Graduate School.

arrangements over the octahedral sites.<sup>10</sup> Therefore, both the A-site cation order and the rock-salt B-site order have a great influence on the properties of  $AA'_3B_2B'_2O_{12}$ . Through the study of  $AA'_3B_2B'_2O_{12}$ , where the A- and B-site are well ordered, it may be possible to study the inhibition of the electron delocalization that led to either Pauli paramagnetism or double-exchange ferromagnetism, while, at the same time, reducing the strength of the superexchange interactions on the octahedral sublattice, thereby enabling a direct study of the  $A'-O-B$  superexchange interactions.

$CaCu_3Cr_4O_{12}$  was synthesized at a pressure of 60 kbar by Subramanian and co-workers.<sup>11</sup> Its crystal structure was determined by X-ray powder diffraction. The compound is cubic with space group  $Im\bar{3}$ <sup>11</sup> and isostructural with  $CaCu_3Mn_4O_{12}$ .<sup>1</sup> Magnetic and electrical measurements show that it is a Pauli-paramagnetic metal.<sup>11</sup> This is different from  $CaCu_3Mn_4O_{12}$ , which is a ferrimagnetic insulator.<sup>1</sup> According to bond valence sums (BVS), the Cu–O and Cr–O bond distances give fractional valences of copper 2.45 and chromium 3.66.<sup>11</sup> This indicates that the valence degeneracy results in metallic properties and a loss of a local moment for copper and chromium. Recently, theoretical study was conducted on  $CaCu_3Cr_4O_{12}$  by the use of the augmented spherical wave (ASW) method within the local spin-density approximation (LSDA).<sup>12</sup> The calculation was performed under both nonspin polarization (NSP) and spin polarization (SP) cases. The results show that the SP ferrimagnetic configuration is more stable compared with the NSP case, contrary to the experimental observation that  $CaCu_3Cr_4O_{12}$  is Pauli paramagnetic.<sup>11</sup> The calculated magnetic moments in  $CaCu_3Cr_4O_{12}$  are chromium 1.41, copper  $-0.16$ , oxygen 0.01, and total  $4.77 \mu_B$ .<sup>12</sup>

On the other hand,  $CaCu_3Cr_2Sb_2O_{12}$  was synthesized at 10 GPa and 1100 °C.<sup>8</sup> The space group  $Pn\bar{3}$  is obtained by X-ray powder diffraction, which is different from  $Im\bar{3}$  of its parent compound,  $CaCu_3Cr_4O_{12}$ .<sup>11</sup> The measured electrical conductivity shows that  $CaCu_3Cr_2Sb_2O_{12}$  is an insulator.<sup>8</sup> By analyzing the temperature dependence of field-cooled magnetization and zero-field-cooled magnetization of  $CaCu_3Cr_2Sb_2O_{12}$  at different magnetic fields, it was found that there exists a ferrimagnetic transition near 160 K.<sup>8</sup> The effective magnetic moment is determined to be  $\sim 1.4 \mu_B$  at 5 K. This indicates that an interaction between A-site Cu(II) and B-site Cr(III) cations is antiferromagnetic and induces the net spontaneous magnetic moment.<sup>8</sup> The effective magnetic moment is significantly smaller than the expected value of  $3 \mu_B$ , estimated assuming an antiparallel alignment of the spins of Cu(II) and Cr(III), which may be due to the spin canting as observed in  $CuCr_2O_4$ .<sup>13</sup> In addition, it is also

interesting to note that among synthesized  $AA'_3B_2B'_2O_{12}$  compounds,<sup>6–9</sup> only  $CaCu_3Cr_2Sb_2O_{12}$  and  $CaCu_3Ga_2M_2O_{12}$  ( $M = Sb, Ta$ )<sup>6</sup> show simultaneous cation ordering on both A- and B-sites in an  $a^+a^+a^+$  perovskite. We are unaware of any theoretical study on  $CaCu_3Cr_2Sb_2O_{12}$ .

In this article, we present a comprehensive study on the magnetic and electronic properties of  $CaCu_3Cr_4O_{12}$  and  $CaCu_3Cr_2Sb_2O_{12}$  by first-principles density functional calculation. The doping of nonmagnetic  $Sb^{5+}$  both dilutes the magnetic ion chromium and induces valence states of chromium from  $Cr^{4+}$  in  $CaCu_3Cr_4O_{12}$  to  $Cr^{3+}$  in  $CaCu_3Cr_2Sb_2O_{12}$ . Thus, it is interesting to investigate the property change upon the doping of  $Sb^{5+}$ . In this aspect, a hypothetical structure  $CaCu_3Cr_2Sn_2O_{12}$ , which is assumed to be isostructural with  $CaCu_3Cr_2Sb_2O_{12}$ , was also studied. In  $CaCu_3Cr_2Sn_2O_{12}$ , the doping of nonmagnetic  $Sn^{4+}$  makes chromium in the 4+ state, as in  $CaCu_3Cr_4O_{12}$ .

## II. Crystal Structures and Computational Method

**A. Structure.** The crystal structures of  $CaCu_3Cr_4O_{12}$  and  $CaCu_3Cr_2Sb_2O_{12}$  are shown in parts a and d of Figure 1. In  $CaCu_3Cr_4O_{12}$ , although all of the Cr–O bond distances are the same (1.926 Å) in  $CrO_6$  octahedra, the O–Cr–O angles are 89.8 and 90.2, instead of 90° in an ideal octahedron. Thus, the  $CrO_6$  octahedra are distorted from the ideal octahedra with  $O_h$  to  $S_6$  symmetry. Distortion is also observed for the  $CuO_4$  unit. The symmetry of  $CuO_4$  is lowered from an ideal planar square with  $D_{4h}$  symmetry to a planar rectangular shape with the pseudo- $D_{4h}$  symmetry. Similar to  $CaCu_3Mn_4O_{12}$ ,<sup>14,15</sup> the  $Cu^{2+}$ , but not the  $Cr^{4+}$  (and  $Mn^{4+}$  in  $CaCu_3Mn_4O_{12}$ ), ion is expected to be the Jahn–Teller ion. The Jahn–Teller ion  $Cu^{2+}$  leads to an oxygen sublattice that corresponds to a tilted 3D network of  $CrO_6$  octahedra. The considerable size mismatch and difference in the bonding requirements for  $Ca^{2+}$  and  $Cu^{2+}$  lead to the deviation of the Cr–O–Cr bond angle ( $140.6^\circ$  in  $CaCu_3Cr_4O_{12}$ ) from an ideal  $180^\circ$  by the tilting of  $CrO_6$  (part c of Figure 1). The space group of  $CaCu_3Cr_4O_{12}$  is  $Im\bar{3}$ .<sup>11</sup> The  $Cu^{2+}$  ion at the 6b site has  $mmm$  symmetry, whereas the chromium ion at the 8c site has  $\bar{3}$  symmetry.

For  $CaCu_3Cr_2Sb_2O_{12}$ , the space group changes from  $Im\bar{3}$  ( $CaCu_3Cr_4O_{12}$ ) to  $Pn\bar{3}$ . The symmetry lowering arises from the replacement of 50% chromium (in  $CaCu_3Cr_4O_{12}$ ) by  $Sb^{5+}$  in an ordered manner (part f of Figure 1).<sup>16</sup> This is consistent with an ordered perovskite structure in an  $a^+a^+a^+$  Glazer tilt system.<sup>17–19</sup> The  $Cu^{2+}$  at the 6d position and the  $Cr^{3+}$  at the 4c position have 222 and  $\bar{3}$  symmetries, respectively. Similar distortion for  $CrO_6$  and  $CuO_4$  units are also observed in  $CaCu_3Cr_2Sb_2O_{12}$ . The tilting of  $CrO_6$  and  $SbO_6$  gives the Cr–O–Sb bond angle of  $139.5^\circ$  (part f of Figure 1).

**B. Methodology.** In the present work, the geometry optimization was performed within the CASTEP code.<sup>20</sup> The Vanderbilt ultrasoft pseudopotential<sup>21</sup> was used with the cutoff energy of 340 eV. The

- (10) Bonnenberg, D.; Boyd, E. L.; Calhoun, B. A.; Folen, V. J.; Grpäer, W.; Greifer, A. P.; Kriessman, C. J.; Lefever, R. A.; McGuire, T. R.; Paulus, M.; Stauss, G. H.; Vautier, R.; Wijn, H. P. J. In *Landolt–Börnstein: Numerical Data and Functional Relationships in Science and Technology*; Hellwege, K. H., Ed.; 1 New Series, Group III; Springer-Verlag: Berlin, 1970; Vol. 4b.
- (11) Subramanian, M. A.; Marshall, W. J.; Calvarese, T. G.; Sleight, A. W. *J. Phys. Chem. Solids* **2003**, *64*, 1569.
- (12) Matar, S. F.; Subramanian, M. A. *Mater. Lett.* **2004**, *58*, 746.
- (13) McGuire, T. R.; Howard, L. N.; Smart, J. D. *Ceram. Age* **1952**, *60*, 22.

- (14) Weht, R.; Pickett, W. E. *Phys. Rev. B* **2001**, *65*, 014415.
- (15) Liu, X. J.; Xiang, H. P.; Cai, P.; Hao, X. F.; Wu, Z. J.; Meng, J. J. *Mater. Chem.* **2006**, *16*, 4243.
- (16) Howard, C. J.; Kennedy, B. J.; Woodward, P. M. *Acta Crystallogr. B* **2003**, *59*, 463.
- (17) Glazer, A. M. *Acta Crystallogr. B* **1972**, *28*, 3384.
- (18) Woodward, P. M. *J. Appl. Crystallogr.* **1997**, *30*, 206.
- (19) Aleksandrov, K. S.; Misjul, S. V. *Sov. Phys. Crystallogr.* **1981**, *26*, 612.
- (20) Segall, M. D.; Lindan, P. L. D.; Probert, M. J.; Pickard, C. J.; Hasnip, P. J.; Clark, S. J.; Payne, M. C. *J. Phys. Condensed Matter* **2002**, *14*, 2717.
- (21) Vanderbilt, D. *Phys. Rev. B* **1990**, *41*, 7892.

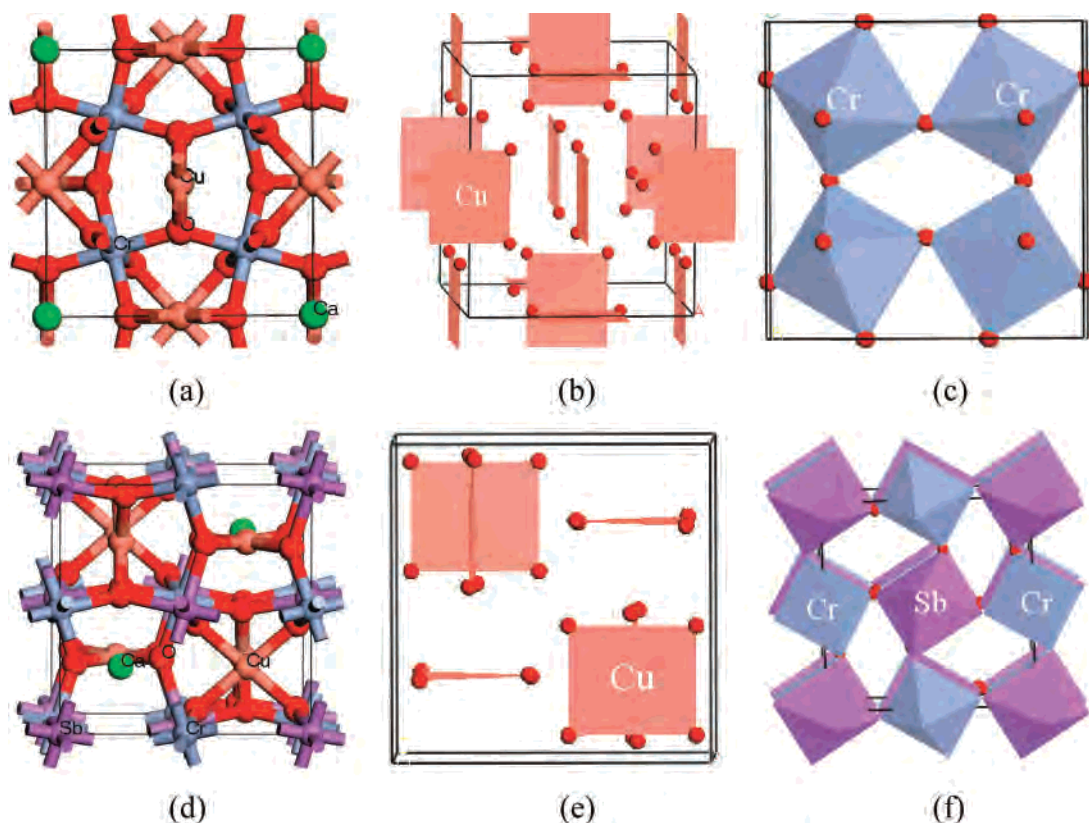


**Figure 1.** (Color online) Crystal structures of (a)  $\text{CaCu}_3\text{Cr}_4\text{O}_{12}$  and (d)  $\text{CaCu}_3\text{Cr}_2\text{Sb}_2\text{O}_{12}$ . (b) and (e) show the  $\text{CuO}_4$  square plane where copper is not shown. (c) and (f) show the octahedra of  $\text{CrO}_6$  and  $\text{SbO}_6$ .

exchange and correlation functionals were treated by the generalized gradient approximation in the formulation of Perdew, Burke, and Ernzerhof (GGA-PBE).<sup>22</sup> The unit cell containing two formula units was fully relaxed, until the self-consistent field convergence per atom, tolerances for total energy, root-mean-square (rms) displacement of atoms, rms force on atoms, and rms stress tensor were less than  $1.0 \times 10^{-6}$  eV,  $1.0 \times 10^{-5}$  eV, 0.001 Å, 0.03 eV/Å, and 0.05 GPa, respectively. The calculations of magnetic and electronic properties were performed using *WIEN2K* program.<sup>23,24</sup> Infinite lattice systems are modeled using periodic boundary conditions. Therefore, it is ideally suitable for calculations on periodic systems. This program is based on the density functional theory and uses the full-potential linearized augmented plane wave (FP-LAPW) method with the dual basis set. In the (L) APW method, the space is divided into atomic spheres and the interstitial region. Then the electronic states are classified as the core states, which are fully contained in the atomic spheres and the valence states. The valence states are expanded using the basis functions. Each of the basis functions has the form of the plane wave in the interstitial region, which is an atomic-like function, as in the atomic spheres. To make the treatment of two valence functions with the same angular momenta (such as 3p and 4p functions of chromium) possible, the so-called local orbitals are added to the basis functions. In our calculation, GGA-PBE was used for the exchange correlation potential.<sup>22</sup> In  $\text{CaCu}_3\text{Cr}_4\text{O}_{12}$ , the muffin-tin radii ( $R_{\text{MT}}$ ) is considered to be equal to 2.41, 1.91, 1.92, and 1.70 bohr for calcium, copper,

chromium, and oxygen, respectively. In  $\text{CaCu}_3\text{Cr}_2\text{Sb}_2\text{O}_{12}$ , the  $R_{\text{MT}}$  are 2.42, 1.96, 1.93, 1.92, and 1.70 bohr for calcium, copper, chromium, antimony, and oxygen, respectively. The plane-wave expansion cutoffs are 7.0 for expanding the wave function (RKMAX) and 14 for expanding the densities and potentials (GMAX) in both compounds. Because the total energy of the ground-state and the magnetic moment is sensitive to the number of k-points used in calculation, we calculated the total energy and magnetic moments with the k-points 200, 300, 400, 500, 600, 800, and 1000. The results suggest that when the k-point is set to be 800 and 500 for  $\text{CaCu}_3\text{Cr}_4\text{O}_{12}$  and  $\text{CaCu}_3\text{Cr}_2\text{Sb}_2\text{O}_{12}$ , respectively, the total energy is the lowest, whereas the magnetic moment does not change much from 200 to 1000 for the two compounds. So in this study, we use the 800 and 500 k-point for  $\text{CaCu}_3\text{Cr}_4\text{O}_{12}$  and  $\text{CaCu}_3\text{Cr}_2\text{Sb}_2\text{O}_{12}$  in the complete Brillouin zone, and the Brillouin zone integration is carried out with a modified tetrahedron method.<sup>25</sup> The self-consistent calculations were considered to be converged when the energy convergence is less than  $10^{-5}$  Ry.

### III. Results and Discussion

**A.  $\text{CaCu}_3\text{Cr}_4\text{O}_{12}$ .** The geometry optimization was performed on  $\text{CaCu}_3\text{Cr}_4\text{O}_{12}$  under both NSP and SP cases. From Table 1, it can be seen that the total energy ( $E_{\text{tot}}$ ) under SP is lower than that under NSP by 1623.6 meV. This result is in agreement with the previous theoretical study that the magnetic configuration is more stable with respect to NSP one.<sup>12</sup> Therefore, only the results from SP are given below.

The calculated magnetic moments are chromium: 1.70, copper:  $-0.47$ , oxygen:  $-0.09$ , and total net magnetic

(22) Perdew, J. P.; Burke, K.; Ernzerhof, M. *Phys. Rev. Lett.* **1996**, *77*, 3865.

(23) Schwarz, K.; Blaha, P. *Comput. Mater. Sci.* **2003**, *28*, 259.

(24) Blaha, P.; Schwarz, K.; Madsen, G. K. H.; Kvasnicka, D.; Luitz, J. *Computer code WIEN2K, An augmented plane waves+local orbitals program for calculating crystal properties*, revised edition 2001; Vienna University of Technology: Vienna, Austria, 2003.

(25) Blöchl, P. E. *Phys. Rev. B* **1994**, *50*, 17953.

**Table 1.** Calculated Total Energy Per Formula Unit (f.u.)  $E_{\text{tot}}$  (eV/f.u.) and Energy Differences  $\Delta E$  (meV/f.u.) between Non- (NSP) and Spin Polarization (SP) Cases, and Magnetic Moment  $\mu_{\text{B}}$  (Bohr Magnetron) of  $\text{CaCu}_3\text{Cr}_4\text{O}_{12}$  and  $\text{CaCu}_3\text{Cr}_2\text{Sb}_2\text{O}_{12}$ 

		$E_{\text{tot}}$ (eV/f.u.)		$\Delta E$ (meV/f.u.)	$\mu_{\text{B}}$			
		NSP	SP		Cu	Cr	O	total
$\text{CaCu}_3\text{Cr}_4\text{O}_{12}$	this work	-20 203.0776	-20 204.7012	1623.6	-0.47	1.70	-0.09	5.0
	theor <sup>a</sup>				-0.16	1.41	-0.01	4.77
$\text{CaCu}_3\text{Cr}_2\text{Sb}_2\text{O}_{12}$	this work	-15 569.5582	-15 572.6017	3043.5	-0.5	2.25	-0.05	3.0
	expt <sup>b</sup>							1.4

<sup>a</sup> Ref 12, theoretical study by ASW within LSDA. <sup>b</sup> Ref 8.

moment:  $5.0 \mu_{\text{B}}$  (Table 1). These values are slightly larger than the previous theoretical values chromium: 1.41; copper:  $-0.16$ ; oxygen:  $-0.01$ , and total:  $4.77 \mu_{\text{B}}$ .<sup>12</sup> Compared with the ideal spin magnetic moments of  $2 \mu_{\text{B}}$  for  $\text{Cr}^{4+}$  ( $S = 1$ ) and  $1 \mu_{\text{B}}$  for  $\text{Cu}^{2+}$  ( $S = 1/2$ ), the calculated values are smaller. The calculated spin magnetic moments indicate that in  $\text{CaCu}_3\text{Cr}_4\text{O}_{12}$ , Cu–Cr is antiferromagnetically coupled, whereas Cu–Cu and Cr–Cr are ferromagnetically coupled. Thus, similar to the experimental observation in  $\text{CaCu}_3\text{Mn}_4\text{O}_{12}$ ,<sup>1,14,15</sup>  $\text{CaCu}_3\text{Cr}_4\text{O}_{12}$  is a ferrimagnetic compound, in agreement with the previous theoretical study.<sup>12</sup> Nonetheless, because  $\text{CaCu}_3\text{Cr}_4\text{O}_{12}$  is reported to be a Pauli-paramagnetic metal by experiment,<sup>11</sup> more research is necessary to solve the discrepancy.

The energy band structure of  $\text{CaCu}_3\text{Cr}_4\text{O}_{12}$  is shown in part a of Figure 2. Metallic behavior is observed for the spin-up channel, whereas semiconducting behavior is seen for the spin-down channel with a direct energy gap of 0.137 eV located at the H point, indicating that  $\text{CaCu}_3\text{Cr}_4\text{O}_{12}$  is half-metallic. This is different from  $\text{CaCu}_3\text{Mn}_4\text{O}_{12}$ , which is an insulator.<sup>1,14,15</sup> From part a Figure 2, we also noted that for the spin-up channel, chromium 3d ( $t_{2g}$ ) electrons occupy mainly around the Fermi energy level and are rather dispersive. This indicates that chromium 3d electrons are itinerant. For copper, the 3d electrons in  $d_{z^2}$ ,  $d_{x^2-y^2}$ ,  $d_{xz}$ , and  $d_{yz}$  orbitals occupy below  $-0.8$  eV. The three empty bands in the energy region from 0.8 to 1.2 eV belong to the unoccupied copper  $d_{xy}$  state. For the spin-down channel, the copper  $d_{xy}$  orbital has three bands at the valence band maximum. The 12 empty bands in the energy region from 0.2 to 2.0 eV are from the unoccupied chromium  $t_{2g}$  state.

The total density of states (TDOS) in part a of Figure 3 show that at the Fermi level ( $E_{\text{F}}$ ) the thermally induced current is 100% spin polarized, which is the unique character for the half metallic compound. From the partial DOS (PDOS) shown in part a of Figure 3, it is seen that at the spin-up channel, the bands at  $E_{\text{F}}$  are mainly from the hybridization between chromium  $t_{2g}$  with oxygen  $p_x$  and  $p_y$  orbitals. For the chromium site, the distorted  $\text{CrO}_6$  octahedra decompose the five 3d orbitals into a nondegenerate  $3z^2-r^2$ , doubly degenerate  $\{x^2-y^2, xy\}$ , and doubly degenerate  $\{xz, yz\}$ . This is the same as in  $\text{CaCu}_3\text{Mn}_4\text{O}_{12}$ .<sup>14,15</sup> The PDOS (part a of Figure 3) show that the 3d orbitals are occupied mainly in the spin-up channel, whereas at the spin-down channel, they are nearly unoccupied. The four orbitals  $\{xz, yz\}$  and  $\{xy, x^2-y^2\}$  are nearly degenerate. The population on the  $d_{z^2}$  orbital is small.

For copper, at the spin-down channel, the 3d orbitals dominate the top of the valence band and hybridize with oxygen  $p_x$  and  $p_y$  orbitals. This is similar to the situation in  $\text{CaCu}_3\text{Mn}_4\text{O}_{12}$ .<sup>14,15</sup> The copper  $d_{xz}$  and  $d_{yz}$  orbitals are located nearly at the same energy region, indicating that they are degenerate. The remaining three orbitals are nondegenerate. This demonstrates that the distorted  $\text{CuO}_4$  unit has the pseudo- $D_{4h}$  symmetry. The  $d_{z^2}$ ,  $d_{x^2-y^2}$ ,  $d_{xz}$ , and  $d_{yz}$  orbitals lie in the energy region from  $-3.0$  to  $-0.8$  eV and are almost completely occupied in both the spin-up channel and the spin-down channel, whereas the  $d_{xy}$  state is located in an energy region just below the Fermi energy level and occupied only in the spin-down channel. In the  $\text{CuO}_4$  unit, copper  $d_{xy}$  and oxygen p orbitals form the d–p $\sigma$  antibonding interactions, similar to the  $d_{x^2-y^2}$  orbital observed in the layered cuprates. In addition, it can be seen that near the  $E_{\text{F}}$ , copper  $d_{xy}$  and chromium 3d orbitals form an antiferromagnetic coupling, in agreement with the calculated spin magnetic moments (Table 1).

**B.  $\text{CaCu}_3\text{Cr}_2\text{Sb}_2\text{O}_{12}$ .** As in  $\text{CaCu}_3\text{Cr}_4\text{O}_{12}$ , the crystal structure of  $\text{CaCu}_3\text{Cr}_2\text{Sb}_2\text{O}_{12}$  was optimized under both NSP and SP cases. From Table 1, it can be seen that the total energy ( $E_{\text{tot}}$ ) under SP is lower than that under NSP by 3043.5 meV. Therefore, only the results under SP are presented.

Similar to  $\text{CaCu}_3\text{Cr}_4\text{O}_{12}$ , the calculated spin magnetic moments (Table 1) show that Cr–Cu is antiferromagnetically coupled, whereas Cu–Cu and Cr–Cr are ferromagnetically coupled. The net magnetic moment is  $3.0 \mu_{\text{B}}$ , indicating that  $\text{CaCu}_3\text{Cr}_2\text{Sb}_2\text{O}_{12}$  is a ferrimagnetic compound. The calculated net magnetic moment of 3.0 is in agreement with the expected value of  $3.0 \mu_{\text{B}}$ , estimated from an antiparallel alignment of the spins of Cu(II) and Cr(III), but larger than the experimentally determined effective magnetic moment of  $\sim 1.4 \mu_{\text{B}}$ .<sup>8</sup> This is probably because the canted spins induce a spontaneous magnetization and lead to a small value in experiment.<sup>8</sup> Because it is difficult to determine the spin canting angle by the theoretical method, future experimental study by neutron diffraction is necessary. The calculated magnetic moments are 2.25 and  $-0.50 \mu_{\text{B}}$  for chromium and copper, respectively, also smaller than the ideal values of  $3 \mu_{\text{B}}$  for  $\text{Cr}^{3+}$  ( $S = 3/2$ ) and  $1 \mu_{\text{B}}$  for  $\text{Cu}^{2+}$  ( $S = 1/2$ ). Nonetheless, our calculation confirmed that  $\text{CaCu}_3\text{Cr}_2\text{Sb}_2\text{O}_{12}$  is a ferrimagnetic compound, in agreement with the experimental observation.<sup>8</sup>

From the band structures shown in part b of Figure 2, it is seen that the calculated band gaps are 0.136 for the spin-up channel and 0.989 eV for the spin-down channel. Both

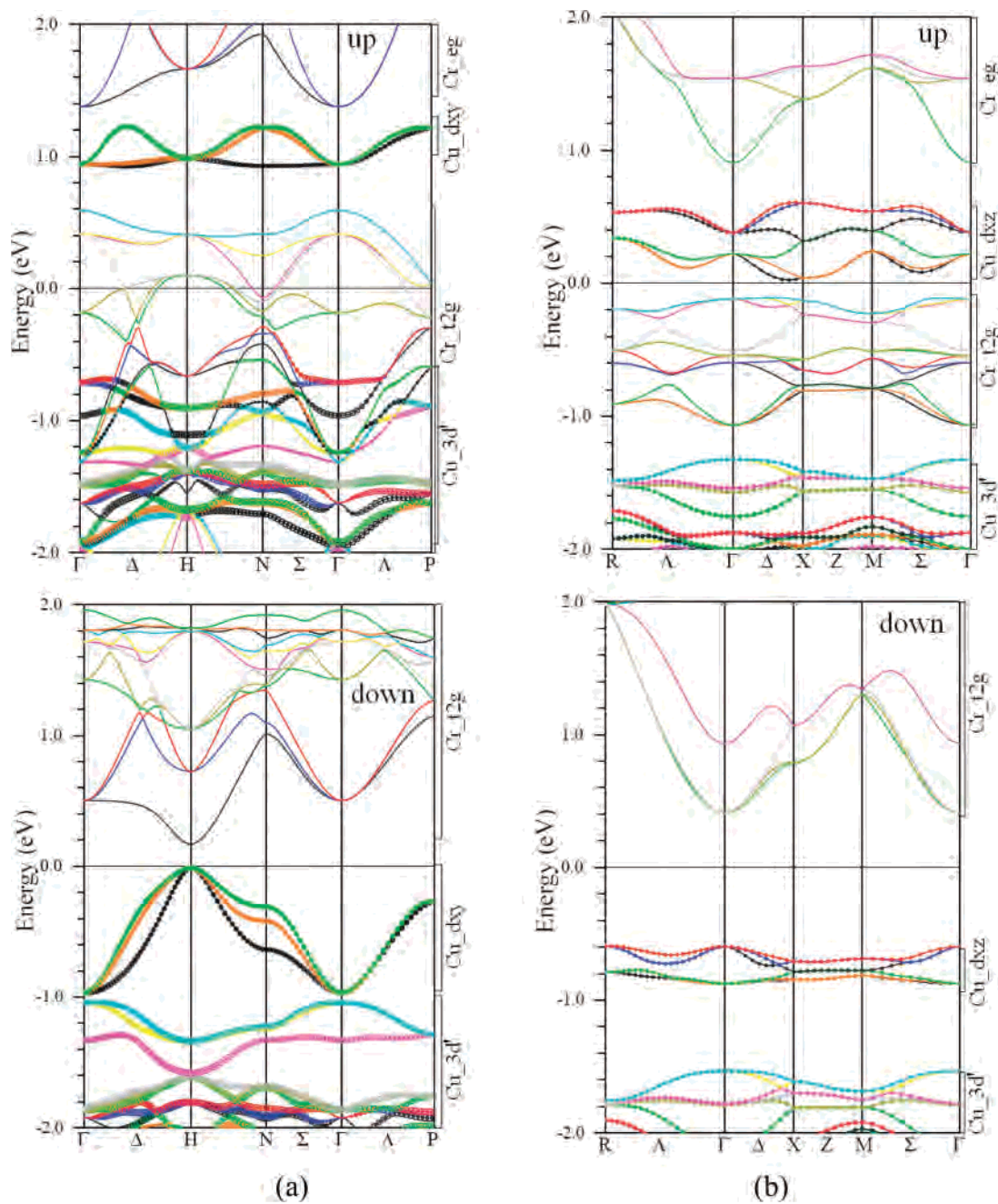


**Figure 2.** (Color online) Band structures near the Fermi energy for spin-up (upper panel) and spin-down (lower panel) channels, (a) CaCu<sub>3</sub>Cr<sub>4</sub>O<sub>12</sub>, (b) CaCu<sub>3</sub>Cr<sub>2</sub>Sb<sub>2</sub>O<sub>12</sub>. Copper 3d bands are plotted by the big dots. Cu\_3d' indicates  $d_{z^2}$ ,  $d_{x^2-y^2}$ ,  $d_{yz}$ , and  $d_{xz}$  in CaCu<sub>3</sub>Cr<sub>4</sub>O<sub>12</sub>;  $d_{z^2}$ ,  $d_{x^2-y^2}$ ,  $d_{xy}$ , and  $d_{yz}$  in CaCu<sub>3</sub>Cr<sub>2</sub>Sb<sub>2</sub>O<sub>12</sub>. The energy region from the specific orbitals is labeled on the outside of the figure. Chromium 3d orbitals are roughly classified as  $t_{2g}$  and  $e_g$ . The energy bands of oxygen overlap with those of the metal atoms. The energy at zero indicates the Fermi energy level.

are indirect. This result is in agreement with the experimental result that the compound is nonmetallic.<sup>8</sup> For the spin-up channel, the valence bands from  $-1.1$  to  $-0.2$  eV are from the hybridization of chromium  $t_{2g}$  with oxygen p orbitals (part b of Figure 2 and part b of Figure 3). The copper 3d electrons in  $d_{z^2}$ ,  $d_{x^2-y^2}$ ,  $d_{xy}$ , and  $d_{yz}$  orbitals mainly occupy below  $-1.3$  eV. There are six empty bands in the energy region from  $0.0$  to  $0.6$  eV, corresponding to the unoccupied copper  $d_{xz}$  state. The four empty bands in the energy region from  $0.9$  to  $2.0$  eV are from the unoccupied chromium  $e_g$  state hybridizing with oxygen p orbitals. For the spin-down channel, the bands from  $-0.8$  to  $-0.6$  eV are from the

hybridization of copper  $dxz$  with oxygen p orbitals. The four empty bands from  $0.4$  to  $2.0$  eV belong to the unoccupied chromium  $t_{2g}$  state. On the other hand, from part b of Figure 3, it is evident that the spin-up and down channels are not symmetric, displaying the character of ferrimagnetic behavior. Compared with CaCu<sub>3</sub>Mn<sub>4</sub>O<sub>12</sub> (refs 14 and 15) and CaCu<sub>3</sub>Cr<sub>4</sub>O<sub>12</sub>, where copper 3d ( $d_{xy}$ ) orbitals are at the valence band maximum, for CaCu<sub>3</sub>Cr<sub>2</sub>Sb<sub>2</sub>O<sub>12</sub>, the copper 3d ( $d_{xz}$ ) orbitals shift away from the Fermi energy level to the lower energy and tend to be localized. The PDOS of copper 3d orbitals show that  $d_{z^2}$ ,  $d_{x^2-y^2}$ ,  $d_{xy}$ , and  $d_{yz}$  orbitals, which are nearly completely occupied both in the spin-up channel

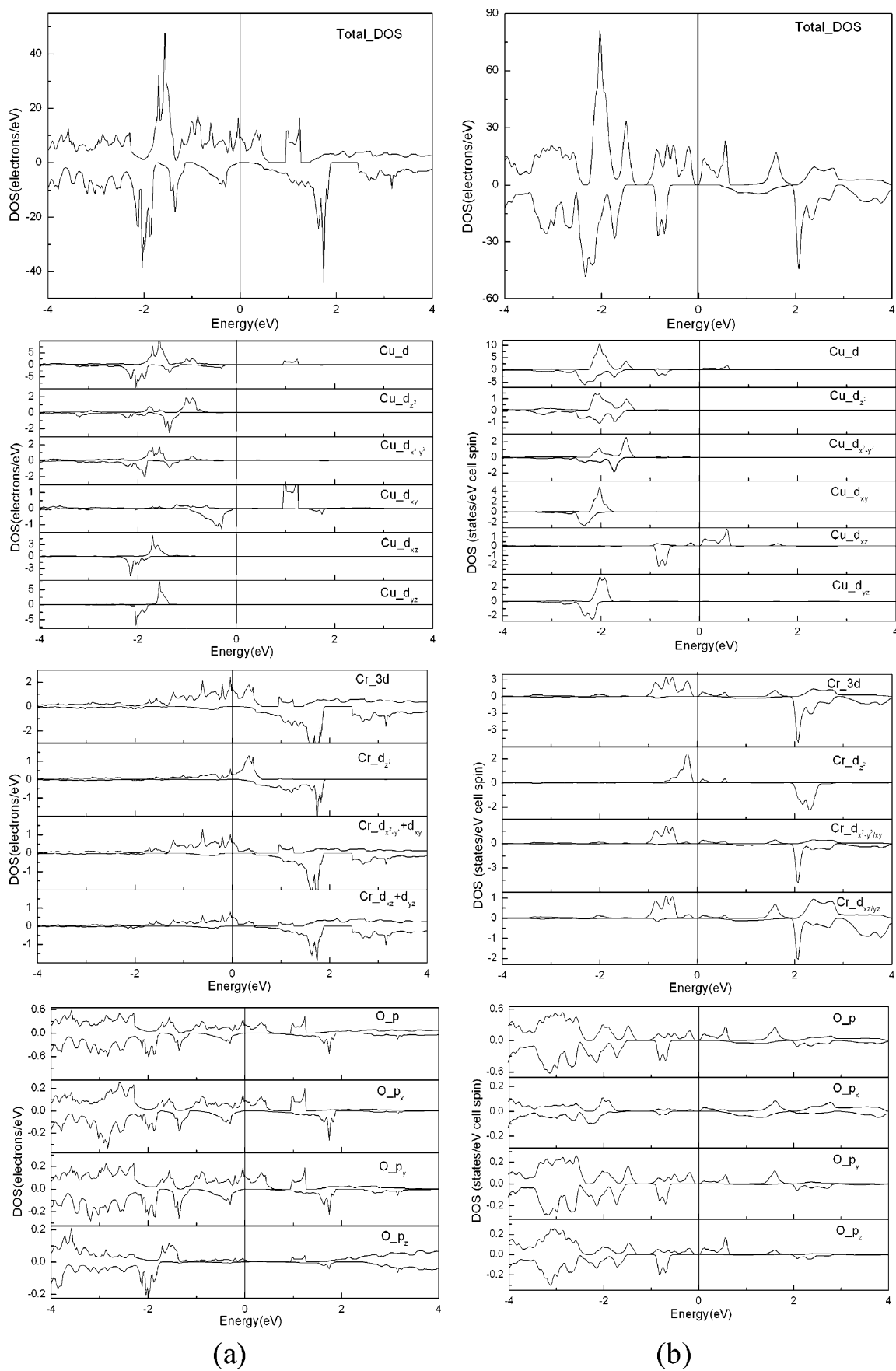


**Figure 3.** Total and partial density of states for (a)  $\text{CaCu}_3\text{Cr}_4\text{O}_{12}$ , (b)  $\text{CaCu}_3\text{Cr}_2\text{Sb}_2\text{O}_{12}$ . The energy at zero indicates the Fermi energy level.

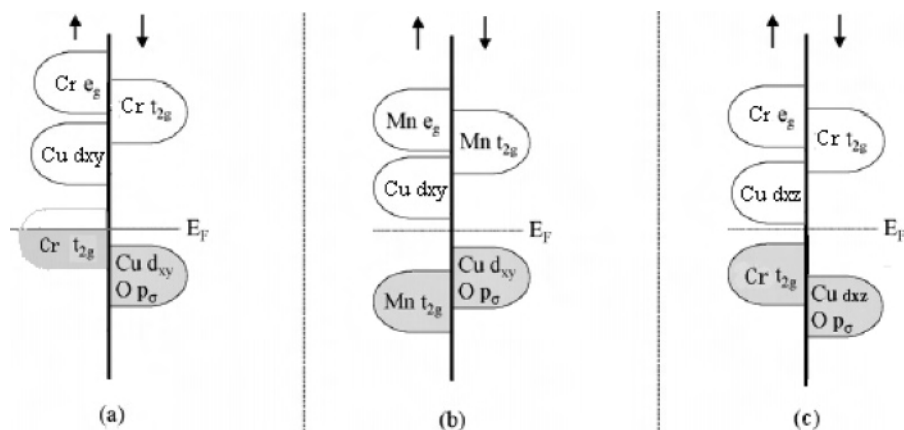


**Figure 4.** Schematic representations of the electronic bands around the Fermi energy level for (a)  $\text{CaCu}_3\text{Cr}_4\text{O}_{12}$ , (b)  $\text{CaCu}_3\text{Mn}_4\text{O}_{12}$ , and (c)  $\text{CaCu}_3\text{Cr}_2\text{Sb}_2\text{O}_{12}$ .

and in the spin-down channel, lie in the energy region from  $-3.0$  to  $-1.3$  eV. The  $d_{xz}$  state is in a higher energy region from  $-0.8$  to  $-0.6$  eV, and occupied only in the spin-down channel. This result is in agreement with the negative effective magnetic moment  $-0.50 \mu_B$  of copper. The chromium 3d orbitals occupy mainly in the spin-up channel. The chromium  $d_{x^2-y^2}$ ,  $d_{xy}$ ,  $d_{xz}$ , and  $d_{yz}$  orbitals from the distorted  $\text{CrO}_6$  octahedron are strongly mixed or degenerate and localized compared with those in  $\text{CaCu}_3\text{Cr}_4\text{O}_{12}$ . In the energy region from  $-0.8$  to  $-0.6$  eV, the copper  $d_{xz}$  and chromium  $d_{xz/yz}$ ,  $d_{xy/x^2-y^2}$  orbitals form an antiferromagnetic superexchange interaction through the oxygen ion.

**C. Magnetic Coupling and Electronic Properties.** The magnetic coupling in  $\text{CaCu}_3\text{Cr}_4\text{O}_{12}$  is quite complex to unravel due to the two types of magnetic ions and local sites with low symmetry. It was previously observed that only Cu–Cu antiferromagnetic coupling exists in  $\text{CaCu}_3\text{Ti}_4\text{O}_{12}$  because titanium is in  $d^0$  configuration.<sup>26,27</sup> The exchange coupling is through the  $\text{TiO}_6$  octahedron.<sup>26,27</sup> Later, the magnetic coupling in the isostructural compound  $\text{CaCu}_3\text{Mn}_4\text{O}_{12}$  was investigated.<sup>14,15</sup> It was found that in  $\text{CaCu}_3\text{Mn}_4\text{O}_{12}$ , the Cu–Cu geometry is the same as that in  $\text{CaCu}_3\text{Ti}_4\text{O}_{12}$ , and the Cu–Cu coupling is through the  $\text{MnO}_6$  octahedron. However, contrary to  $\text{Ti}^{4+}$  with  $d^0$  configuration in  $\text{CaCu}_3\text{Ti}_4\text{O}_{12}$ ,  $\text{Mn}^{4+}$  with  $d^3$  configuration in  $\text{CaCu}_3\text{Mn}_4\text{O}_{12}$  provides different magnetic coupling in that the Mn–Mn is antiferromagnetic and Cu–Cu is ferromagnetic. Because of the reduction of the Mn–O–Mn bond angle from  $180^\circ$  to  $142^\circ$ , the parallel alignment of the manganese spin is observed, that is, the coupling of Mn–Mn is ferromagnetic. Because  $\text{CaCu}_3\text{Cr}_4\text{O}_{12}$  is isostructural with  $\text{CaCu}_3\text{Mn}_4\text{O}_{12}$ , the interaction of Cu–Cu in  $\text{CaCu}_3\text{Cr}_4\text{O}_{12}$  is through the  $\text{CrO}_6$  octahedron, similar to that in  $\text{CaCu}_3\text{Mn}_4\text{O}_{12}$  through the  $\text{MnO}_6$  octahedron. Moreover, the electronic configuration of  $\text{Cr}^{4+}$  ( $d^2$ ) is similar to that of  $\text{Mn}^{4+}$  ( $d^3$ ), in which 3d electrons are less than half filled. Therefore, the  $\text{CrO}_6$  octahedron plays the same role as  $\text{MnO}_6$ . That is, in  $\text{CaCu}_3\text{Cr}_4\text{O}_{12}$ , Cu–Cr coupling is antiferromagnetic, whereas Cu–Cu is ferromagnetic. According to Goodenough–Kanamori–Anderson rules,

$\text{Cr}^{4+}\text{–O–Cr}^{4+}$  ( $d^2\text{–}d^2$ ) coupling with an angle of  $180^\circ$  is antiferromagnetic (viz.  $\text{CaCrO}_3$ ,  $\text{Cr}^{4+}$ ).<sup>28</sup> When the angle is reduced to the range of  $125^\circ\text{–}150^\circ$ , a ferromagnetic coupling is expected.<sup>28</sup> This is in agreement with our conclusion, that is, the Cr–O–Cr angle is  $140.6^\circ$  and Cr–Cr is ferromagnetically coupled. The above discussion suggests that, for  $\text{CaCu}_3\text{B}_4\text{O}_{12}$  ( $B = 3d$  transition metal), the electronic configuration of B ions and the B–O–B angle play important roles in the magnetic couplings of Cu–B, Cu–Cu, and B–B. Our recent prediction on  $\text{CaCu}_3\text{Fe}_4\text{O}_{12}$  also supported the above conclusion.<sup>29</sup> In  $\text{CaCu}_3\text{Fe}_4\text{O}_{12}$ , iron is in a  $4+$  state, and the Fe–O–Fe angle is  $139.1^\circ$ . The coupling of Cu–Fe is antiferromagnetic, whereas that of Cu–Cu and Fe–Fe is ferromagnetic.<sup>29</sup>

Parts a and b of Figure 4 show the schematic representation of the electronic bands around the Fermi level for  $\text{CaCu}_3\text{Cr}_4\text{O}_{12}$  and  $\text{CaCu}_3\text{Mn}_4\text{O}_{12}$ . In insulating  $\text{CaCu}_3\text{Mn}_4\text{O}_{12}$ , the manganese  $t_{2g}$  band is half filled ( $d^3$ ), and the conductivity can be thermally activated. For  $\text{CaCu}_3\text{Cr}_4\text{O}_{12}$ , chromium  $t_{2g}$  has only two electrons ( $d^2$ ) less than half filled. This makes chromium 3d electrons delocalized, tends to strengthen ferromagnetic interaction of Cr–Cr through oxygen, and results in the Cr–O–Cr network being conductive. This can be observed from the electronic density map of the (010) plane of the spin-up channel for  $\text{CaCu}_3\text{Cr}_4\text{O}_{12}$  (part a of Figure 5). Thus, metallic behavior is expected to occur for one of the spin channels and is indeed observed in the band structures (the spin-up channel in this study, part a of Figure 2). Therefore, for  $\text{CaCu}_3\text{Cr}_4\text{O}_{12}$ , the electronic configuration of  $\text{Cr}^{4+}$  ( $d^2$ ) with  $t_{2g}$  less than half filled ( $d^3$ ) will strengthen Cr–Cr ferromagnetic interaction.

Similar to  $\text{CaCu}_3\text{Cr}_4\text{O}_{12}$ , the magnetic coupling in  $\text{CaCu}_3\text{Cr}_2\text{Sb}_2\text{O}_{12}$  is also quite complex. In the compound, the magnetic ions  $\text{Cr}^{3+}$  are diluted by nonmagnetic ion  $\text{Sb}^{5+}$  in an ordered manner. Hence, Cr–Cr superexchange coupling in the octahedral network is reduced significantly compared with that in  $\text{CaCu}_3\text{Cr}_4\text{O}_{12}$ . The interaction of Cu–Cu is through the  $\text{CrO}_6$  ( $\text{Cr}^{3+}$ ,  $d^3$ ) octahedron. The Cr–Cu anti-

(26) Lacroix, C. *J. Phys. C* **1980**, *13*, 5125.

(27) Collomb, A.; Samaras, D.; Bochu, B.; Joubert, J. C. *Phys. Status Solidi A* **1977**, *41*, 459.

(28) Goodenough, J. *Magnetism and the Chemical Bond*; Wiley-Interscience: New York, 1996.

(29) Xiang, H. P.; Liu, X. J.; Zhao, E. J.; Meng, J.; Wu, Z. J.; *Appl. Phys. Lett.* **2007**, *91*, 011903.

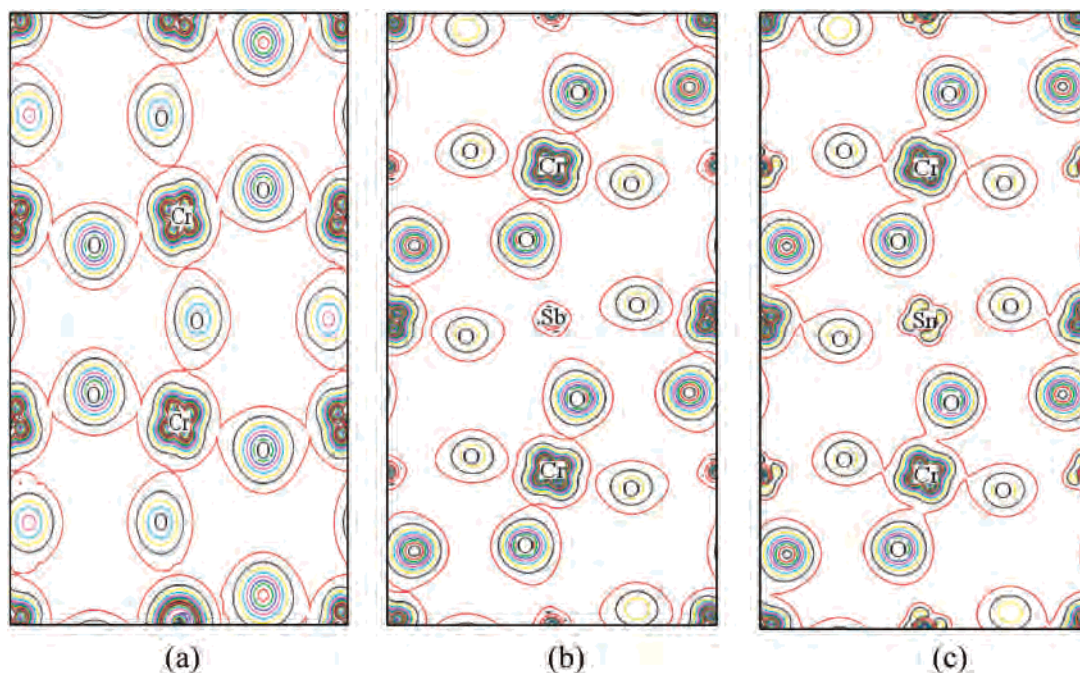


**Figure 5.** (Color online) Electronic density maps of the (010) plane of spin-up for (a)  $\text{CaCu}_3\text{Cr}_4\text{O}_{12}$ , (b)  $\text{CaCu}_3\text{Cr}_2\text{Sb}_2\text{O}_{12}$ , and (c)  $\text{CaCu}_3\text{Cr}_2\text{Sn}_2\text{O}_{12}$ , respectively.

ferromagnetic coupling and Cu–Cu ferromagnetic coupling exist in  $\text{CaCu}_3\text{Cr}_2\text{Sb}_2\text{O}_{12}$ . Parts b and c of Figure 4 show the schematic representation of the electronic bands around the Fermi level for  $\text{CaCu}_3\text{Mn}_4\text{O}_{12}$  and  $\text{CaCu}_3\text{Cr}_2\text{Sb}_2\text{O}_{12}$ . In  $\text{CaCu}_3\text{Cr}_2\text{Sb}_2\text{O}_{12}$ , the  $\text{Cr}^{3+}$  3d has three electrons with  $t_{2g}$  half filled ( $t_{2g}^3$ ), and there is a band gap around the Fermi level as that in  $\text{CaCu}_3\text{Mn}_4\text{O}_{12}$  ( $\text{Mn}^{4+} t_{2g}^3$ ). The larger band gap of  $\text{CaCu}_3\text{Cr}_2\text{Sb}_2\text{O}_{12}$  (0.136 eV) compared with that of  $\text{CaCu}_3\text{Mn}_4\text{O}_{12}$  (0.09 eV)<sup>14</sup> indicates that, the doping of nonmagnetic ion  $\text{Sb}^{5+}$ , which reduces the Cr–Cr ferromagnetic coupling significantly, might be responsible for the weakening of the conductivity in  $\text{CaCu}_3\text{Cr}_2\text{Sb}_2\text{O}_{12}$ . Therefore, for  $\text{CaCu}_3\text{B}_4\text{O}_{12}$  (B = 3d transition metal), the conductivity of  $\text{CaCu}_3\text{B}_4\text{O}_{12}$  could be reduced by the doping of nonmagnetic ion B' at the B site in an ordered manner.

From  $\text{CaCu}_3\text{Cr}_4\text{O}_{12}$  to  $\text{CaCu}_3\text{Cr}_2\text{Sb}_2\text{O}_{12}$ , the doping of nonmagnetic ion  $\text{Sb}^{5+}$  induces the valence state of chromium from +4 to +3. Therefore, to get further insight into the influence of the valence states of chromium and nonmagnetic ion  $\text{Sb}^{5+}$  on the physical properties, we studied the electronic structure of a hypothetical compound,  $\text{CaCu}_3\text{Cr}_2\text{Sn}_2\text{O}_{12}$ , by assuming the structure of  $\text{CaCu}_3\text{Cr}_2\text{Sb}_2\text{O}_{12}$  through replacing the  $\text{Sb}^{5+}$  with  $\text{Sn}^{4+}$ . In  $\text{CaCu}_3\text{Cr}_2\text{Sn}_2\text{O}_{12}$ , chromium has the same valence state, +4, as in the  $\text{CaCu}_3\text{Cr}_4\text{O}_{12}$ , but different from +3 in  $\text{CaCu}_3\text{Cr}_2\text{Sb}_2\text{O}_{12}$ . Moreover,  $\text{Sn}^{4+}$  is also a nonmagnetic ion. Our calculated results show that, similar to  $\text{CaCu}_3\text{Cr}_4\text{O}_{12}$  and  $\text{CaCu}_3\text{Cr}_2\text{Sb}_2\text{O}_{12}$ ,  $\text{CaCu}_3\text{Cr}_2\text{Sn}_2\text{O}_{12}$  is also a ferrimagnetic compound, and the interaction between copper and chromium is antiferromagnetic. The band structures suggest that  $\text{CaCu}_3\text{Cr}_2\text{Sn}_2\text{O}_{12}$  is a semiconductor with a quite-small thermal gap of 0.008 eV, much smaller than that of  $\text{CaCu}_3\text{Cr}_2\text{Sb}_2\text{O}_{12}$  (0.136 eV). This might be due to the fact that the  $\text{Cr}^{4+} t_{2g}$  orbital in  $\text{CaCu}_3\text{Cr}_2\text{Sn}_2\text{O}_{12}$  is occupied by only two electrons (less than half filled compared with half-filled  $\text{Cr}^{3+} t_{2g}^3$  in  $\text{CaCu}_3\text{Cr}_2\text{Sb}_2\text{O}_{12}$ ), thus

making the electrons in  $\text{CaCu}_3\text{Cr}_2\text{Sn}_2\text{O}_{12}$  less localized and the interaction between chromium and oxygen stronger. This is demonstrated by the electronic density maps of the (010) plane of the spin-up channel for  $\text{CaCu}_3\text{Cr}_2\text{Sb}_2\text{O}_{12}$  and  $\text{CaCu}_3\text{Cr}_2\text{Sn}_2\text{O}_{12}$ , shown in parts b and c of Figure 5. It is seen that the hybridized interaction between chromium and oxygen in  $\text{CaCu}_3\text{Cr}_2\text{Sn}_2\text{O}_{12}$  is stronger than that in  $\text{CaCu}_3\text{Cr}_2\text{Sb}_2\text{O}_{12}$ . On the other hand, as in  $\text{CaCu}_3\text{Cr}_4\text{O}_{12}$ , chromium has valence state of +4 in  $\text{CaCu}_3\text{Cr}_2\text{Sn}_2\text{O}_{12}$ . From parts a and c of Figure 5, it is seen that, compared with  $\text{CaCu}_3\text{Cr}_4\text{O}_{12}$ , the nonmagnetic  $\text{Sn}^{4+}$  ion reduces the Cr–O–Cr superexchange interaction in  $\text{CaCu}_3\text{Cr}_2\text{Sn}_2\text{O}_{12}$ , thus weakening the conductivity of the Cr–O–Cr network, as encountered in  $\text{CaCu}_3\text{Cr}_2\text{Sb}_2\text{O}_{12}$ . Therefore, it is clear that the electronic configuration of  $\text{Cr}^{3+}$  ( $t_{2g}^3$ ) and the doping of nonmagnetic ion  $\text{Sb}^{5+}$  have a great influence on the conducting behavior of  $\text{CaCu}_3\text{Cr}_2\text{Sb}_2\text{O}_{12}$ .

Finally, we compare  $\text{CaCu}_3\text{Cr}_2\text{Sb}_2\text{O}_{12}$  with the other  $\text{CaCu}_3\text{B}_2\text{B}'_2\text{O}_{12}$  compounds. Different from the  $\text{CaCu}_3\text{Cr}_2\text{Sb}_2\text{O}_{12}$ , both  $\text{CaCu}_3\text{Cr}_2\text{Ru}_2\text{O}_{12}$  and  $\text{CaCu}_3\text{Ga}_2\text{Ru}_2\text{O}_{12}$  crystallize in space group  $Im\bar{3}$ , where cations are disordered over the octahedral B site and show Pauli-paramagnetic metallic behavior.<sup>7,9</sup> This may be due to the well-known broadening of the d band when going from the 3d to the 4d series. Moreover, the disorder of the octahedral B sites makes the electrons more delocalized. On the other hand, the pure paramagnetic behavior of  $\text{CaCu}_3\text{Ga}_2\text{M}_2\text{O}_{12}$  (M = Sb, Ta) (with cation ordering on both A- and B-sites),<sup>6</sup> which, contrary to the antiferromagnetic  $\text{CaCu}_3\text{Ti}_4\text{O}_{12}$ ,<sup>26,27</sup> suggests that the magnetic coupling within the A' sublattice is strongly influenced by the electronic configuration of the B, B' sublattice.

$\text{CaCu}_3\text{Cr}_2\text{Sb}_2\text{O}_{12}$  shows simultaneous cation ordering on both A- and B-sites and has 50% magnetic ion  $\text{Cr}^{3+}$  and 50% nonmagnetic ion  $\text{Sb}^{5+}$  at the octahedral B sites. The ordered arrangement of the chromium and antimony and the



nonmagnetic ion  $\text{Sb}^{5+}$  simultaneously inhibits the electron delocalization that leads to either Pauli paramagnetism or double-exchange ferromagnetism, while at the same time reduces the strength of the Cr–Cr superexchange interactions. Thus, compound  $\text{CaCu}_3\text{Cr}_2\text{Sb}_2\text{O}_{12}$  shows ferrimagnetic character, and the spontaneous magnetization is associated with the  $\text{Cu}^{2+}$ – $\text{Cr}^{3+}$  superexchange interaction. Therefore, the ordering arrangement of the octahedral chromium and antimony ions and the electronic configuration of  $\text{Cr}^{3+}$  ( $d^3$ ) play important roles in producing a ferrimagnetic insulating character of  $\text{CaCu}_3\text{Cr}_2\text{Sb}_2\text{O}_{12}$ .

#### IV. Conclusions

$\text{CaCu}_3\text{Cr}_4\text{O}_{12}$  and  $\text{CaCu}_3\text{Cr}_2\text{Sb}_2\text{O}_{12}$  were studied by the use of density functional theory. In  $\text{CaCu}_3\text{Cr}_4\text{O}_{12}$ ,  $\text{CrO}_6$ , in which  $\text{Cr}^{4+}$  3d orbitals have only two electrons ( $d^2$ ) less than half filled ( $d^5$ ), this provides a bridge for the exchange process of Cu–Cu and Cu–Cr, resulting in Cu–Cr antiferromagnetic and Cu–Cu ferromagnetic couplings. Because the angle of Cr–O–Cr,  $140.6^\circ$ , deviates from the ideal  $180^\circ$  significantly,  $\text{Cr}^{4+}$ – $\text{Cr}^{4+}$  is ferromagnetically coupled. Moreover, chromium 3d electrons are delocalized, which makes the Cr–O–Cr network conductive. Therefore,  $\text{CaCu}_3\text{Cr}_4\text{O}_{12}$  shows ferrimagnetic and half-metallic properties. For  $\text{CaCu}_3\text{Cr}_2\text{Sb}_2\text{O}_{12}$ ,  $\text{Cr}^{3+}$  3d orbitals are occupied by three electrons ( $d^3$ ), which are also less than half filled. Thus, similar to  $\text{CaCu}_3\text{Cr}_4\text{O}_{12}$ ,

Cu–Cr is antiferromagnetically coupled, whereas Cu–Cu is ferromagnetically coupled. However, as a result of the doping of nonmagnetic ion  $\text{Sb}^{5+}$ , the magnetic ions  $\text{Cr}^{3+}$  are diluted. Hence,  $\text{Cr}^{3+}$ – $\text{Cr}^{3+}$  ferromagnetic coupling is significantly reduced in comparison with that in  $\text{CaCu}_3\text{Cr}_4\text{O}_{12}$ . Moreover,  $\text{Cr}^{3+}$  with the  $t_{2g}$  orbitals half filled ( $t_{2g}^3$ ) leads the chromium 3d electrons to be localized, which reduces further the interaction of  $\text{Cr}^{3+}$ – $\text{Cr}^{3+}$ . In addition, the ordering arrangement of the octahedral chromium and antimony ions also prohibits the delocalization of electrons. Therefore,  $\text{CaCu}_3\text{Cr}_2\text{Sb}_2\text{O}_{12}$  is a ferrimagnetic semiconductor with an energy gap of 0.136 eV. These results suggest that for  $\text{CaCu}_3\text{B}_4\text{O}_{12}$  (B = 3d transition metal), the electronic configuration of B ions play an important role in tailoring the conducting properties and the magnetic couplings of Cu–B, Cu–Cu, and B–B. If B 3d orbitals are populated but less than half filled ( $d^n$ ,  $n < 5$ ), the coupling of Cu–B could be antiferromagnetic, whereas those of Cu–Cu and B–B are ferromagnetic. The doping of nonmagnetic ion B' at B site in an ordered manner could weaken the conductivity of  $\text{CaCu}_3\text{B}_4\text{O}_{12}$ .

**Acknowledgment.** The authors thank the National Natural Science Foundation of China (NSFC) for financial support (Grants 20571073, 20331030, and 20601026).

IC070213Q